Frequency-domain crosswell reverse time migration with up and downgoing wave separation

Yike Liu, Huiyi Lu, Institute of Geology and Geophysics, Chinese Academy of Sciences; Youli Quan, Stanford University; Xiao-Bi Xie, University of California at Santa Cruz*

Summary

Crosswell reverse time migration (RTM) with up and downgoing wave separation can greatly reduce artifacts usually seen in the conventional RTM without wave separation. However, the up and downgoing wave separation cannot be efficiently conducted in space-time domain algorithms because the upper/lower half space images are indistinguishable. In order to tackle this problem, we propose a frequency-domain algorithm with up and downgoing wave decomposition for the crosswell RTM. The numerical experiments and field data example demonstrate that the proposed method can greatly attenuate migration artifacts while still keep reasonable efficiency.

Introduction

Surface seismic data has insufficient resolution to determine vertical and horizontal extents of a reservoir. For accurately identifying the boundary and fine structures of a reservoir, geophysicists often employ downhole seismic techniques where sources and geophones are emplaced close to the deeply buried targets and beneath highly complex surface layers. An important downhole imaging method is the crosswell tomography. Transmission data from crosswell seismic surveys are tomographically inverted for velocity and attenuation structures (Peterson et al., 1985; Luo and Schuster, 1991; Quan and Harris, 1997) to delineate moderate-sized details (down to 5 meters in many cases) of channel sands and reservoir layers. The main problem with traveltime tomography is that it typically suffers from limited spatial resolution of no better than about 5 meters, partially due to the high-frequency asymptotic approximation inherent in the ray theory. To improve the resolution, CDP stack of crosswell reflection signals has been proven a useful tool for imaging interwell structures. Once the primary reflections are effectively extracted from the data, VSP-CDP mapping (Harris et al., 1995; Lazaratos et al., 1995) or Kirchhoff prestack constrained migration (Schuster, 1993, Qin & Schuster, 1993; Cai & Schuster, 1993; Zhou et al., 1995; Nemeth et al., 1997; Zheng, 2005) can usually generate satisfactory crosswell images of simple structures. When the interwell structures become more complex, however, problems may arise with the Kirchhoff migration method, e.g., unable to generate true amplitude images for crosswell reservoir characterization. To solve the amplitude preserving problem, the RTM is introduced to image crosswell data.

RTM emerged as a very powerful and general imaging tool for reflection seismology since early 1980s (Baysal et al., 1983; Whitmore, 1983; Chang and McMechan, 1987; Deng and McMechan, 2008). RTM is based on two-way wave equation and exhibits great superiority over other imaging algorithms in handling steeply dipping structures, complicated velocity models and is able to preserve wave amplitude. Unlike the Kirchhoff migration (Liner and Lines ,1993; Liu et al., 2007), the conventional RTM is implemented gather by gather, which cannot differentiate upper and lower half space images. As a result, the upper space reflection creates a fake mirror reflection in the lower space, and vice versa. To reduce the artifacts generated due to the upper/lower half space imaging, the migration needs to be implemented in a trace by trace style and separates the up and downgoing waves. Although this can be easily done under the framework of the Kirchhoff migration, it is incredibly expensive using a conventional time-domain RTM. In order to improve crosswell RTM, we propose the frequency-domain RTM for crosswell data including up and downgoing wave separation. This method can greatly attenuate mirror artifacts while still keep the reasonable efficiency.

Methodology

The frequency-domain full-wave equation can be expressed as (Marfurt, 1984)

$$\mathbf{S}\tilde{\mathbf{g}}(\omega,\vec{x};\vec{x}_s)=\boldsymbol{\delta}(\vec{x}-\vec{x}_s), \tag{1}$$

where

$$\mathbf{S}=\mathbf{K}+i\omega\mathbf{C}+\omega^2\mathbf{M} \tag{2}$$

is the complex impedance matrix composed of stiffness matrix **K**, damping matrix **C** and the mass matrix **M,** $\tilde{\mathbf{g}}(\omega,\vec{x},\vec{x}_s)$ is the Green function which is the wavefield generated by an impulse source $\boldsymbol{\delta}(\vec{x}-\vec{x}_s)$ located at $\vec{x}_s$, and $i=\sqrt{-1}$. All these quantities are functions of spatial position $\vec{x}$ and the angular frequency ω.

RTM can be considered as the zero-lag cross correlation between the forward propagated source wavefield and the backward propagated receiver wavefield. For RTM imaging, the source wavefield $\tilde{\mathbf{p}}$ can be expressed as the convolution (multiplication in frequency domain) of the Green function and the source vector **f**

DOI http://dx.doi.org/10.1190/segam2013-0132.1

$$\tilde{\mathbf{p}}(\omega,\vec{x},\vec{x}_s)=\tilde{\mathbf{g}}(\omega,\vec{x},\vec{x}_s)\mathbf{f}(\omega,\vec{x}_s)\cdot \quad (3)$$

Similarly, the receiver wavefield can be expressed as

$$\tilde{\mathbf{b}}(\omega,\vec{x};\vec{x}_r,\vec{x}_s)=\tilde{\mathbf{g}}(\omega,\vec{x};\vec{x}_r)\mathbf{d}(\omega,\vec{x}_r,\vec{x}_s), \quad (4)$$

where $\mathbf{d}$ is the trace record at $\vec{x}_r$ generated by the source at $\vec{x}_s$. Correlating the source and the receiver wavefields, we have the migration image for a single source-receiver pair

$$I(\omega,\vec{x};\vec{x}_r,\vec{x}_s)=\tilde{\mathbf{p}}(\omega,\vec{x};\vec{x}_s)\tilde{\mathbf{b}}^*(\omega,\vec{x};\vec{x}_r,\vec{x}_s), \quad (5)$$

where the asterisk denotes the complex conjugate, which is equivalent to the time reversion in time domain. The final image can be obtained by summing up partial images for all sources, receivers and frequencies

$$I(\vec{x})=\sum_{\omega=0}^{\omega_{\max}}\sum_{s=1}^{N_s}\sum_{r=1}^{Nr} I\ (\omega,\vec{x};\vec{x}_r,\vec{x}_s). \quad (6)$$

Based on the above derivations, crosswell RTM with up and downgoing wave separation can be summarized as follows:

(1) FK filtering the frequency domain receiver data $\mathbf{d}(\omega,\vec{x}_r,\vec{x}_s)$ to separate it into up and downgoing data $\mathbf{d}_{up}(\omega,\vec{x}_r,\vec{x}_s)$ and $\mathbf{d}_{down}(\omega,\vec{x}_r,\vec{x}_s)$, where subscripts *up* and *down* are for up and downgoing wavefields.

(2) The up and downgoing receiver wavefields from a single trace can be calculated as follows

$$\tilde{\mathbf{b}}^*_{down}(\omega,\vec{x};\vec{x}_r,\vec{x}_s)=\tilde{\mathbf{g}}(\omega,\vec{x};\vec{x}_r)\mathbf{d}^*_{down}(\omega,\vec{x}_r,\vec{x}_s), \quad (7)$$

$$\tilde{\mathbf{b}}^*_{up}(\omega,\vec{x};\vec{x}_r,\vec{x}_s)=\tilde{\mathbf{g}}(\omega,\vec{x};\vec{x}_r)\mathbf{d}^*_{up}(\omega,\vec{x}_r,\vec{x}_s). \quad (8)$$

(3) Use the following imaging condition with up and downgoing wave separation for all shots and frequencies

$$I(\vec{x})=\sum_{\omega=0}^{\omega_{\max}}\sum_{s=1}^{N_s}\sum_{r=1_r}^{N_r}\{\tilde{\mathbf{p}}_s(\omega,\vec{x};\vec{x}_s)\}^T\begin{cases}\tilde{\mathbf{b}}_{down}(\omega,\vec{x};\vec{x}_r,\vec{x}_s) & \text{for } \vec{x} \text{ above } \vec{x}_r\\ \tilde{\mathbf{b}}_{up}(\omega,\vec{x};\vec{x}_r,\vec{x}_s) & \text{for } \vec{x} \text{ below } \vec{x}_r\end{cases}. \quad (9)$$

The RTM in equation 9 is composed of cross correlations between the forward propagated source wavefield and the up and down going back propagated receiver wavefields. In each grid point, Green functions are calculated for all receivers and sources. An upgoing wave is selected for imaging if the image point is located below the receiver level. On the contrary, if a grid point is above the receiver level, downgoing wave will be used for imaging. Compared to the conventional time-domain crosswell RTM, the proposed frequency-domain algorithm with wave separation can greatly reduce computational cost and significantly attenuate imaging artifacts.

Numerical examples

To illustrate the frequency-domain crosswell RTM with up and downgoing wave separation, a 3-layer velocity model shown in Figure 1 is discretized onto a 100 x 200 mesh with intervals of 2 m, where the two interfaces are located at depths 50 and 300 m, and associated velocities are 1800 m/s, 3000 m/s and 1800 m/s, respectively. A single synthetic shot record is generated by a frequency-domain acoustic-wave forward modeling, with 124 traces separated by an interval of 2 m. Each trace has 2501 samples with a sampling interval of 0.08 ms. The direct waves are muted from the synthetic data.

To demonstrate the proposed crosswell RTM with up and downgoing wave separation, we implement imaging at 66 frequencies from 0 to 200 Hz with an increment of 0.305 Hz. The source is a Ricker wavelet with a dominant frequency of 100 Hz. Instead of using all 124 traces, we give two examples, one with a single trace and the other with 7 traces, which let us clearly see the effectiveness to attenuate artifacts generated due to upper or lower half spaces indistinguishable.

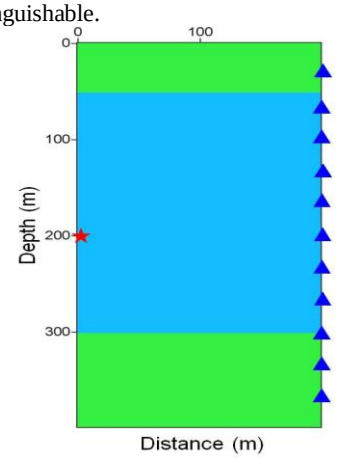

Figure 1: A three-layer velocity model. The velocities from top to bottom are 1800 m/s, 3000 m/s and 1800 m/s, respectively. The star and triangles are locations of source and receivers.

Figure 2 shows the crosswell images from a single trace, where the source and receiver are placed at the same depth of z=200 m. The long axis of each ellipse is along a line connecting the source and receiver. The two interfaces are imaged well at the depths 50 m and 300 m, labeled I1 and I2, respectively. However, there are strong artifacts at depths 100 m and 350 m (labeled I1' and I2' in Figure 2a), which are caused by mirror reflections. After using equation 9, these artifacts are successfully removed by wave separation (Figure 2b).

DOI http://dx.doi.org/10.1190/segam2013-0132.1

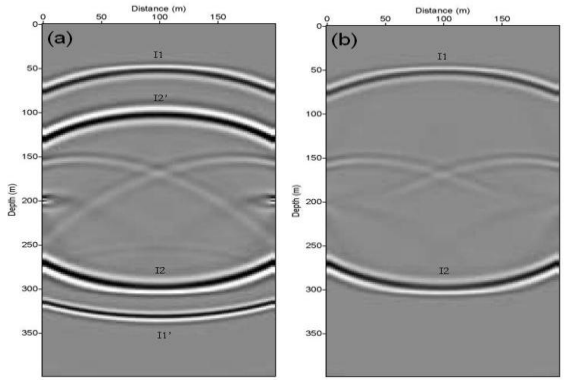

Figure 2: (a) Image from a single trace without up and downgoing wave separation. (b) Similar to (a) but with wave separation. I1' is the mirror reflection of interface I1, and I2' is the mirror reflection of interface I2.

To further demonstrate the validity of equation 9, the number of traces is increased to 7 with an increment of 40 m. There are multiple ellipses related to the source and 7 corresponding receivers (Figure 3a). Most of them are artifacts due to that the conventional RTM fails to distinguish between upper and lower half spaces. The 4 artifacts located between depths 300 m and 400 m are generated by the 4 lower traces in the receiver well, and other 3 large-angle artifacts between 50 m and 300 m are associated with the 3 shallow traces. The results show, without wave separation, there are 7 upper half space elliptical artifacts generated by imaging the interface at 300 m depth. These artifacts will strongly affect the image quality, leading to wrong geological interpretations. After up and downgoing wave separation and using the image equation 9, most of these mirror artifacts can be removed as shown in Figure 3b.

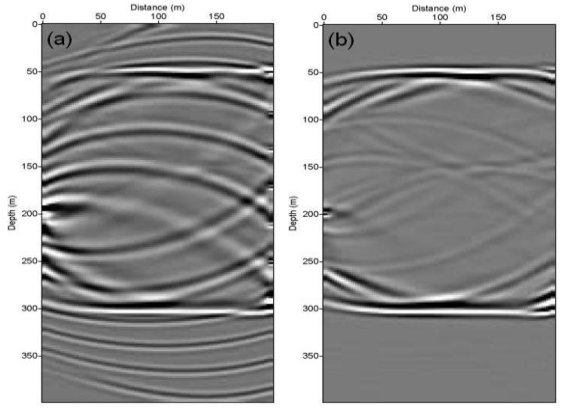

Figure 3: (a) Image using 7 traces without up and downgoing wave separation. (b) Similar to (a) but after up and downgoing wave separation.

Field data example

We test the crosswell RTM with up and downgoing wave separation on a west Texas data set. There are 201 shots evenly distributed along the well from depth 2500 *m* to 2800 *m*, with a source interval of 1.5 *m*. For all common shot gathers, 203 hydrophones are evenly distributed from depth 2500 *m* to 2800 *m*, with a trace interval of 1.5 *m*. The offset between the wells is 198 *m*, and the velocity model is discretized into a (133,206) grid, with a grid size of 1.5 *m* x 1.5 *m*. The velocity model obtained from ray tracing tomography is shown in Figure 4. Several prominent features are easily identified in the tomogram and can be correlated with logs. The background velocities colored by green are related to some low-velocity zones at the depth 2590 m to 2640 m and 2652 to 2743 m closing to the well B, while the lowest velocity appears between 2775 and 2804 ft, just below a region with the highest velocity.

A set of preprocessing has been applied to the crosswell data. In order to avoid spatial aliasing in the final image, a 300-2000 Hz band pass filter was applied to the raw data in the common shot gather. The direct, tube and shear waves have been removed before migration of the reflected P waves. The tube waves are suppressed by using a median filter. The shear wave muting was based on the shear time picking, and all waves arrived later than the shear wave would be cut off. In order to separate the up-going and down-going waves, an FK filer was applied to the data, where the frequency passband is 300-1500 Hz.

After the above processing, the data was migrated to the image domain using the frequency RTM with up and down going wave separation (Figure 5). The reflection image has much better vertical resolution than the tomogram and add complementary small scale details to the tomogram. Several reflection events with subtle and obvious variations in character can be seen at the range from the depth 2560 to 2580 and 2630 to 2660 m, respectively. Many of these events carry across from well to well and may correspond to the continuous reservoir horizons. Perhaps a striking feature of the reflection image occurs close to the lower right part of the model, where a visible delineation of wedges can be found near the depth from 2750 to 2770 m. This range of depths corresponds to the relatively high-velocity zone in the tomogram. The strata above this depth are gradually dipping from right to left with a slope of more than 15 degrees which shows an angular unconformity. This dipping feature is easily identified with the reflection image than from the tomogram, but only with the crosswell reflection images.

DOI http://dx.doi.org/10.1190/segam2013-0132.1

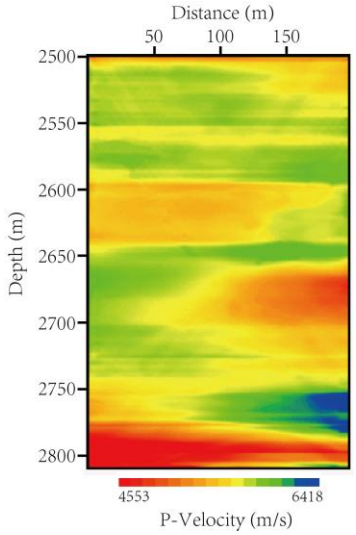

Figure 4: Velocity model for RTM imaging obtain by traveltime tomography.

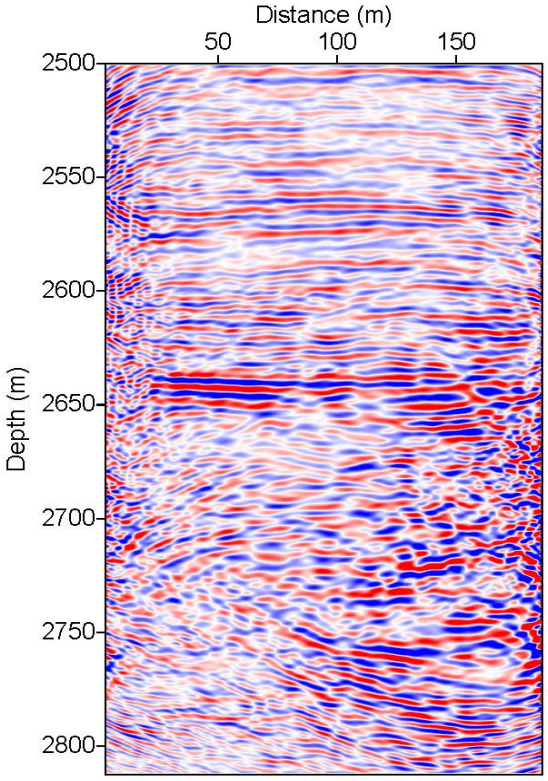

Figure 5: The reverse time migration image with up and down going wave separation for crosswell data.

Conclusions

RTM has the advantage of providing fine-scale features with true amplitude for crosswell data processing. After separating the up and downgoing waves, we propose a frequency-domain crosswell RTM, which can greatly attenuate the image artifacts generated by mirror reflections. As a frequency-domain method, we pre-calculate and store the Green functions for all sources and receivers, and use them repeatedly. To store Green functions for one frequency is more practical than to store the entire time series, and the frequency-domain multiplication in wavefield reconstruction are more efficient than the time-domain convolution. Put these together, the efficiency of the proposed method is comparable to the conventional time-domain RTM.

Acknowledgements

We would like to thank Jerry M. Harris and Yingcai Zheng for fruitful discussions. The research was partially supported by the National Nature Science Foundation of China (Grant. 40930421, 41074091) and the National Oil and Gas Projects of China (2011ZX05008-006).

I

DOI http://dx.doi.org/10.1190/segam2013-0132.1

http://dx.doi.org/10.1190/segam2013-0132.1

EDITED REFERENCES

Note: This reference list is a copy-edited version of the reference list submitted by the author. Reference lists for the 2013 SEG Technical Program Expanded Abstracts have been copy edited so that references provided with the online metadata for each paper will achieve a high degree of linking to cited sources that appear on the Web.

REFERENCES

Baysal, E., D. Kosloff, and J. Sherwood, 1983, Reverse time migration: Geophysics, **48**, 1514–1524.

Cai, W., and G. T. Schuster, 1993, Processing Friendswood crosswell seismic data for reflection imaging: 63rd Annual International Meeting, SEG, Expanded Abstracts, 92–94.

Chang, W. F., and G. A. McMechan, 1987, Elastic reverse-time migration: Geophysics, **52**, 1365–1375, http://dx.doi.org/10.1190/1.1442249.

Deng, F., and G. A. McMechan, 2008, Viscoelastic true-amplitude prestack reverse-time depth migration: Geophysics, **73**, no. 4, S143–S155, http://dx.doi.org/10.1190/1.2938083.

Harris, J., R. Nolen-Hoeksema, R. Langan, M. van Schaack, S. Lazaratos, and J. Rector III, 1995, High-resolution crosswell imaging of a west Texas carbonate reservoir: Part l - project summary and interpretation: Geophysics, **60**, 667–681, http://dx.doi.org/10.1190/1.1443806.

Lazaratos, S., J. Rector, J. M. Harris, and M. V. Schaack, 1995, High resolution crosswell imaging of a west Texas carbonate reservoir: 65th Annual International Meeting, SEG, Expanded Abstracts, 49–53.

Liner, C. L., and L. R. Lines, 1993, Simple prestack migration of cross-well seismic data: 63rd Annual International Meeting, SEG, Expanded Abstracts, 308–311.

Liu, Y., H. Sun, and X. Chang, 2007, Crosswell imaging by two-dimensional oriented wave path migration: Geophysical Journal International, **169**, 233–239, http://dx.doi.org/10.1111/j.1365-246X.2006.03281.x.

Luo, Y., and G. T. Schuster, 1991, Wave equation traveltime inversion: Geophysics, **56**, 645–653, http://dx.doi.org/10.1190/1.1443081.

Marfurt, K., 1984, Accuracy of finite-difference and finite-element modeling of the scalar and elastic wave equation: Geophysics, **49**, 533–549, http://dx.doi.org/10.1190/1.1441689.

Nemeth, T., E. Normark, and F. Qin, 1997, Dynamic smoothing in crosswell traveltime tomography: Geophysics, **62**, 168–176, http://dx.doi.org/10.1190/1.1444115.

Peterson, J., B. Paulsson, and T. McEvilly, 1985, Applications of algebraic reconstruction techniques to crosshole seismic data: Geophysics, **50**, 1566–1580, http://dx.doi.org/10.1190/1.1441847.

Qin, F., and G. T. Schuster, 1993, Constrained Kirchhoff migration of crosswell seismic data: 63rd Annual International Meeting, SEG, Expanded Abstracts, 99–102.

Quan, Y., and J. Harris, 1997, Seismic attenuation tomography using the frequency shift method: Geophysics, **62**, 895–905, http://dx.doi.org/10.1190/1.1444197.

Schuster, G. T., 1993, Least-squares cross-well migration: 63rd Annual International Meeting, SEG, Expanded Abstracts, 110–113.

Whitmore, N. D., 1983, Iterative depth migration by backward time propagation: 53rd Annual International Meeting, SEG, Expanded Abstracts, 382–385.

Zheng, Y., and X. Tang, 2005, Imaging near-borehole structure using acoustic logging data with pre-stack F-K migration: 75th Annual International Meeting, SEG, Expanded Abstracts, 360–363.

Zhou, C., W. Cai, Y. Luo, G. T. Schuster, and S. Hassanzadeh, 1995, Acoustic wave equation traveltime and waveform inversion of crosshole seismic data: Geophysics, **60**, 765–773, http://dx.doi.org/10.1190/1.1443815.